LETTER TO THE EDITOR

The P132H mutation in the main protease of Omicron SARS-CoV-2 decreases thermal stability without compromising catalysis or small-molecule drug inhibition

© CEMCS, CAS 2022

Cell Research (2022) 32:498–500; https://doi.org/10.1038/s41422-022-00640-y

Dear Editor,

The ongoing SARS-CoV-2 pandemic continues to be a significant threat to global health. First reported in November 2021, the Omicron variant (B.1.1.529) is more transmissible and can evade immunity better than previous SARS-CoV-2 variants, fueling an unprecedented surge in cases. To produce functional proteins from its polyprotein, SARS-CoV-2 relies on the cysteine proteases Nsp3/papain-like protease (PL^{pro}) and Nsp5/main protease (M^{pro})/3C-like protease to cleave at three and more than 11 sites, respectively.[1] Therefore, M^{pro} and PL^{pro} inhibitors are considered to be one of the most promising SARS-CoV-2 antivirals. On December 22, 2021, the Food and Drug Administration (FDA) issued an Emergency Use Authorization (EUA) for PAXLOVID, a ritonavir-boosted formulation of nirmatrelvir. Nirmatrelvir is a first-in-class orally bioavailable SARS-CoV-2 M^{pro} inhibitor.[2] Thus, the scientific community must vigilantly monitor potential mechanisms of drug resistance, especially because SARS-CoV-2 is naïve to M^{pro} inhibitors. Mutations have been well identified in variants to this point.[3] Notably, Omicron M^{pro} (OM^{pro}) harbors a single mutation—P132H. In this study, we characterized the enzymatic activity, drug inhibition, and structure of OM^{pro} while evaluating the past and future implications of M^{pro} mutations.

Using an established Förster resonance energy transfer (FRET) assay to monitor proteolytic activity,[4] we show that OM^{pro} and wild-type (WT) M^{pro} have equivalent affinity and catalytic constants for its substrate (Fig. 1a, b). However, subsequent melting temperature experiments reveal OM^{pro} has a melting temperature (T_m) of 53.6 ± 0.1 °C; lower than the WT M^{pro} T_m of 56.2 ± 0.2 by 2.6 °C (Fig. 1b). Despite its lower melting temperature, OM^{pro} and WT M^{pro} hydrolyze their substrates at comparable rates for up to 24 h at 37 °C (Fig. 1c). Further biochemical analysis suggests that OM^{pro} and M^{pro} are equally susceptible to covalent inhibitors such as GC-376, PF-07321332 (nirmatrelvir), and PF-00835231 (Fig. 1d). Interestingly, when these inhibitors are incubated with WT M^{pro} or OM^{pro}, their melting temperatures converge, despite the different melting temperature of their apo forms (Fig. 1e). This suggests that inhibitors may stabilize OM^{pro} to a greater extent than WT M^{pro}. These described biochemical/biophysical results are in line with the equivalent antiviral potency of these molecules against WT and Omicron and the lack of observable differences in the active site.[5–8]

In parallel to our study, Ullrich et al. also characterized six M^{pro} mutants identified from the circulating SARS-CoV-2 variants.[9] The catalytic efficiency (k_{cat}/K_m) values for WT and Omicron M^{pro} were 0.016 and 0.023 s^{-1} μM^{-1}, similar to the values obtained in our study (Fig. 1b). In addition, the Pfizer team reported that PF-07321332 (nirmatrelvir) retained a potent inhibitory constant (K_i) against Omicron P132H M^{pro} (K_i = 0.635 nM), similar to WT (K_i = 0.933 nM).[10] Our independent study further confirmed these results.

The crystal structure of OM^{pro} in complex with GC-376 was determined at 2.05 Å resolution in the monoclinic space group I2 with a R_{work}/R_{free} of 0.179/0.219 (Supplementary information, Table S1; PDB ID 7TOB). The unit cell is the same as many previously solved WT M^{pro} crystal structures where a = 45.19 Å, b = 52.99 Å, c = 113.01 Å and α = 90.00°, β = 100.50°, γ = 90.00°. Overall, OM^{pro} has a nearly identical structure to WT M^{pro} (Fig. 1f).[4] The most pronounced differences involve the area around the mutation associated with OM^{pro}, P132H. Found 22 Å from the catalytic cysteine Cys145, P132H lies between the catalytic domain and the dimerization domain, and thus, it does not impart any direct structural changes to the active site.

Clear electron density shows that His132 forms π-stacking interactions with the sidechain of Glu240 (Fig. 1g). As the imidazole sidechain of histidine is protonated near physiological pH, the interaction with Glu240 may be further strengthened through electrostatic interactions. Additionally, there is a newly formed water-mediated hydrogen bond with Glu240. We also find that Glu240 reorients itself toward the core to accommodate the bulkier His sidechain, where it forms a new hydrogen bond with Thr198 (Fig. 1h). Consequently, the Thr198 sidechain rotates ~90°, placing its hydroxyl group in close distance to Glu240. As a result of these conformational changes, certain portions of the enzyme appear to move very slightly, ~0.5 Å (Fig. 1f). We speculate that the lower thermal stability of apo OM^{pro} may be due to minor residue adjustments to accommodate the bulkier His132 sidechain, ultimately destabilizing its structure. Because the mutation occurs at the interface between the dimerization domain and the catalytic domain, these movements can also affect intramolecular packing. Residue 132 is also located at the turn between two β-sheets, a position that naturally favors the cyclic sidechain of proline.

Although the P132H mutation does not appear to reduce enzymatic activity and inhibitor binding (Fig. 1a–d), the decrease in thermal stability (Fig. 1b) indicates that protein flexibility may be greater, which plays an important role in enzyme evolution, especially to broaden substrate profile or to alter ligand binding. M^{pro} can recognize a wide range of peptide substrates, although its P1 position preferentially binds to glutamine. Future studies on whether P132H and other mutations can influence enzymatic activity for larger substrate libraries or other known ligands will be necessary. In addition, the effect of the M^{pro} P132H mutant on the viral replication remains elusive, and further works need to generate recombinant viruses to study the viral replication kinetics and tropism.

Extensive sequencing of SARS-CoV-2 isolates has provided unprecedented insights into the mutations that occur in the viral RNA genome.[3] Based on the annotations provided through CoVsurver enabled by GISAID (www.gisaid.org/epiflu-applications/covsurver-mutations-app), mutations of Nsp5 appear mostly

Received: 26 January 2022 Accepted: 21 February 2022
Published online: 15 March 2022

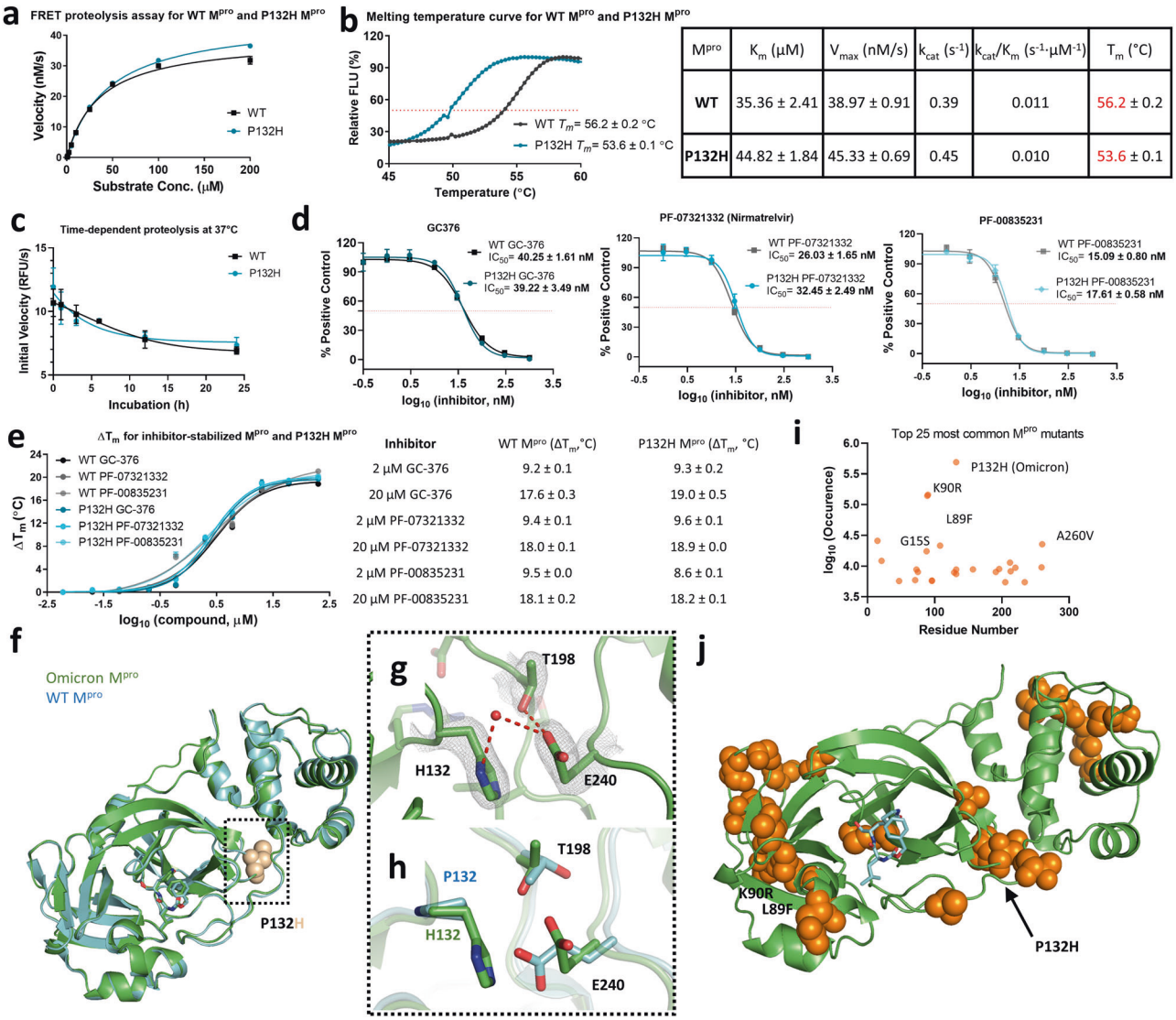

Inhibitor	WT Mpro (ΔTm, °C)	P132H Mpro (ΔTm, °C)
2 μM GC-376	9.2 ± 0.1	9.3 ± 0.2
20 μM GC-376	17.6 ± 0.3	19.0 ± 0.5
2 μM PF-07321332	9.4 ± 0.1	9.6 ± 0.1
20 μM PF-07321332	18.0 ± 0.1	18.9 ± 0.0
2 μM PF-00835231	9.5 ± 0.0	8.6 ± 0.1
20 μM PF-00835231	18.1 ± 0.2	18.2 ± 0.1

Mpro	Km (μM)	Vmax (nM/s)	kcat (s-1)	kcat/Km (s-1·μM-1)	Tm (°C)
WT	35.36 ± 2.41	38.97 ± 0.91	0.39	0.011	56.2 ± 0.2
P132H	44.82 ± 1.84	45.33 ± 0.69	0.45	0.010	53.6 ± 0.1

Fig. 1 Biochemical and structural comparison of WT and Omicron M^{pro} P132H. a Characterization of enzymatic activity shows that WT M^{pro} and Omicron M^{pro} have comparable catalytic activity. **b** Thermal shift assay for apo proteins demonstrates that Omicron M^{pro} has a lower T_m than WT M^{pro} by 2.6 °C. **c** Time-dependent proteolytic activity suggests that substrate turnover in both enzymes decreases at a similar rate when incubated at 37 °C for extended periods of time. **d** Covalent inhibitors GC-376, PF-07321332 (nirmatrelvir), and PF-00835231 are equally potent against WT M^{pro} and Omicron M^{pro}. **e** Likewise, by assessing their ΔT_m as a function of inhibitor concentration, we show that they are both stabilized to a similar extent by GC-376, PF-07321332 (nirmatrelvir), and PF-00835231. **f** Crystal structure of SARS-CoV-2 Omicron M^{pro} + GC-376 at 2.05 Å resolution (green) superimposed with WT M^{pro} + GC-376 (blue; PDB ID 7C6U). P132H is shown as spheres. **g** Electron density map of H132 and surrounding residues. $2F_o$-F_c map is contoured at 1 σ and shown in gray. **h** Structural comparison of position 132 and interacting residues in WT M^{pro} and Omicron M^{pro}. **i** Top 25 most common M^{pro} mutants. **j** Top 25 most common M^{pro} mutants mapped onto the crystal structure of SARS-CoV-2 Omicron M^{pro} as orange spheres. Three most common mutants P132H, K90R, and L89F are labeled.

stochastic (Supplementary information, Fig. S1); however, several positions have a disproportionately large number of mutations. Of the top 25 most common mutants (Fig. 1i), three are found on P132: P132H (489,444 occurrences; EPI_ISL_8931050), P132L (8813 occurrences; EPI_ISL_8768027), and P132S (7452 occurrences; EPI_ISL_8925342). L89F, K90R, and K88R are the second, third, and seventh, most common mutations, suggesting this β-sheet is also a hotspot. Notably, none of the 25 most common mutants involve residues in the active site or at the dimerization interface (Fig. 1j). With several exceptions, including P132H, the resulting amino acid is often similar in size and physicochemical properties, such as K→R. However, SARS-CoV-2 has not yet encountered M^{pro} antivirals. If nothing else, SARS-CoV-2 has taught us that widespread proliferation, low fidelity genome synthesis, and selective pressure might quickly produce drug-resistant phenotypes. Thus, it is important to monitor future mutations and their associated biochemical properties to anticipate future drug-resistance.

Michael Dominic Sacco[1], Yanmei Hu[2], Maura Verenice Gongora[1], Flora Meilleur[3,4], Michael Trent Kemp[1], Xiujun Zhang[1], Jun Wang[2]✉ and Yu Chen[1]✉

[1]*Department of Molecular Medicine, Morsani College of Medicine, University of South Florida, Tampa, FL, USA.* [2]*Department of Medicinal Chemistry, Ernest Mario School of Pharmacy, Rutgers, the State University of New Jersey, Piscataway, NJ, USA.* [3]*Department of Molecular and Structural Biochemistry, North Carolina State University, Raleigh, NC, USA.* [4]*Neutron Scattering Division, Oak Ridge National Laboratory, Oak Ridge, TN, USA.*

✉*email: junwang@pharmacy.rutgers.edu; ychen1@usf.edu*

DATA AVAILABILITY

The X-ray crystal structure of the Omicron M^{pro} P132H mutant in complex with GC376 was deposited in PDB with the code 7TOB.

REFERENCES

1. Cannalire, R. et al. *J. Med. Chem.* https://doi.org/10.1021/acs.jmedchem.0c01140 (2020).
2. Owen, D. R. et al. *Science* **374**, 1586–1593 (2021).
3. WHO. https://www.who.int/en/activities/tracking-SARS-CoV-2-variants Accessed on 19 February 2022. (2022).
4. Ma, C. et al. *Cell Res.* **30**, 678–692 (2020).
5. Dabrowska, A. et al. *bioRxiv* https://doi.org/10.1101/2021.12.21.473268 (2021).
6. Rai, D. K. et al. *bioRxiv* https://doi.org/10.1101/2022.01.17.476644 (2022).
7. Vangeel, L. et al. *Antiviral Res.* **198**, 105252 (2022).
8. Rosales, R. et al. *bioRxiv* https://doi.org/10.1101/2022.01.17.476685 (2022).
9. Ullrich, S. et al. *Boorg. Med. Chem. Lett.* https://doi.org/10.1016/j.bmcl.2022.128629 (2022).
10. Greasley, S. E. et al. *bioRxiv* https://doi.org/10.1101/2022.01.17.476556 (2022).

ACKNOWLEDGEMENTS

X-ray data were collected at the X-ray facility supported by the Spallation Neutron Source (Oak Ridge National Laboratory), a DOE Office of Science User Facility. This research was supported by the National Institutes of Health (NIH) (grants AI147325, AI157046, and AI158775) to J.W. We thank Eric M Lewandowski for reviewing this paper.

AUTHOR CONTRIBUTIONS

M.D.S., J.W., and Y.C. conceived the experiments, interpreted the data, and composed the paper. Y.H. performed the biochemical assays and melting temperature experiments. Proteins were cloned and purified by X.Z. Crystal structures were solved and refined by M.D.S. Crystals were grown by M.V.G. X-ray datasets were prepared and collected by M.T.K and F.M.

COMPETING INTERESTS

The authors declare no competing interests.

ADDITIONAL INFORMATION

Supplementary information The online version contains supplementary material available at https://doi.org/10.1038/s41422-022-00640-y.

Correspondence and requests for materials should be addressed to Jun Wang or Yu Chen.

Reprints and permission information is available at http://www.nature.com/reprints